

RESEARCH

Open Access



# EGb761 suppressed vascular dementia via modulating Wnt/ $\beta$ -catenin signaling pathway-induced apoptosis and autophagy in hippocampal neuronal cells

Nan Yin<sup>1,2,3</sup>, Zhipeng Tang<sup>4</sup>, Yanyan Yang<sup>5</sup>, Xiuqin Li<sup>6</sup>, Ruisheng Duan<sup>2</sup>, Guodong Xu<sup>2</sup> and Peiyuan Lv<sup>1,2,3\*</sup>

## Abstract

**Objectives** The study aimed to explore the effects of EGb761 on vascular dementia (VD) rats and the mechanisms of action.

**Methods** The Morris water maze test was utilized to assess the spatial learning and memory abilities of the rats; Hematoxylin and Eosin (HE) staining and electron microscopy were used to observe changes in hippocampal neuron cells; Immunohistochemistry was performed to detect the expression of cleaved caspase-3 and microtubule-associated proteins light chain 3 (LC3-II) positive cells in hippocampal neurons; immunofluorescence staining was carried out to determine the immunofluorescence intensity of IRGM in hippocampal neurons; western blotting was used to measure the expression of related proteins.

**Results** EGb761 significantly improved the cognitive function of vascular dementia rats ( $P < 0.01$ ) and reduced the apoptosis of hippocampal neurons. Furthermore, EGb761 suppressed ROS, thereby promoting the expression of proteins related to the Wnt/ $\beta$ -catenin signaling pathway and inhibiting the expression of C-Jun N-terminal Kinase (p-JNK), c-Jun N-terminal kinase (p-c-JUN), Protein 53 (P53), immunity-related GTPase M (IRGM), Transcription Factor EB (TFEB), microtubule-associated proteins light chain 3 (LC3), Lysosomal Associated Membrane Protein 1 (LAMP1), and Sequestosome 1 (SQSTM1).

**Conclusions** Ginkgo Biloba Extract 761 (EGb761) mediated the Wnt/ $\beta$ -catenin signaling pathway to inhibit apoptosis and autophagy in hippocampal neurons in VD rats.

**Keywords** Vascular dementia rats, Hippocampal neurons, EGb761, Wnt/ $\beta$ -catenin signaling pathway, Autophagy

\*Correspondence:

Peiyuan Lv  
peiyuanlu2@163.com

<sup>1</sup> Department of Neurology, Hebei Medical University, No. 361 Zhongshan East Road, Shijiazhuang City, Hebei Province 050017, People's Republic of China

<sup>2</sup> Department of Neurology, Hebei General Hospital, No. 348 Heping West Road, Shijiazhuang City, Hebei Province 050051, People's Republic of China

<sup>3</sup> Hebei Provincial Key Laboratory of Cerebral Networks and Cognitive Disorders, Hebei General Hospital, No. 348 Heping West Road, Shijiazhuang City, Hebei Province 050051, People's Republic of China

<sup>4</sup> Department of Laboratory Medicine, Hebei General Hospital, No. 348 Heping West Road, Shijiazhuang City, Hebei Province 050051, People's Republic of China

<sup>5</sup> Department of Gynecology, Hebei General Hospital, No. 348 Heping West Road, Shijiazhuang City, Hebei Province 050051, People's Republic of China

<sup>6</sup> Department of Geriatrics, Hebei General Hospital, No. 348 Heping West Road, Shijiazhuang City, Hebei Province 050051, People's Republic of China



© The Author(s) 2025. **Open Access** This article is licensed under a Creative Commons Attribution-NonCommercial-NoDerivatives 4.0 International License, which permits any non-commercial use, sharing, distribution and reproduction in any medium or format, as long as you give appropriate credit to the original author(s) and the source, provide a link to the Creative Commons licence, and indicate if you modified the licensed material. You do not have permission under this licence to share adapted material derived from this article or parts of it. The images or other third party material in this article are included in the article's Creative Commons licence, unless indicated otherwise in a credit line to the material. If material is not included in the article's Creative Commons licence and your intended use is not permitted by statutory regulation or exceeds the permitted use, you will need to obtain permission directly from the copyright holder. To view a copy of this licence, visit <http://creativecommons.org/licenses/by-nc-nd/4.0/>.

## Introduction

Vascular dementia (VD) is a chronic, acquired, and progressive syndrome involving cognitive impairment caused by various cerebrovascular diseases. Research indicates that VD is the second most prevalent form of dementia globally, following Alzheimer's disease (AD), affecting 1.5% of the Chinese population aged 65 and older. Patients with VD experience a spectrum of symptoms, including neurological deficits and cognitive impairment, which pose severe threats to their physical and mental health and impose a significant economic burden on society and families. The pathogenesis of VD remains incompletely elucidated, and current treatments primarily aim to manage associated cardiovascular risk factors and alleviate accompanying symptoms [1, 2]. Consequently, unraveling the pathogenesis of VD, devising rational treatment strategies, and identifying efficacious therapeutic agents have emerged as focal points in cognitive disorder research.

Clinically, VD is characterized by cognitive impairments intricately linked to aberrations in brain structure and function, as well as atypical cerebral blood flow distributions. Chronic cerebral hypoperfusion (CCH) can induce ischemia, hypoxia, and glucose insufficiency in brain tissue, precipitating oxidative stress, apoptosis, autophagy, and other homeostatic alterations. Cognition-related brain regions and tissues vulnerable to ischemia and hypoxia frequently exhibit chronic hypoperfusion, culminating in delayed neuronal necrosis and cognitive dysfunction, and potentially progressing to dementia. Both apoptosis and autophagy are pivotal for maintaining internal environmental stability and for moderating cellular protein content. These mechanisms are often concurrently activated to regulate programmed cell death during normal growth, stress reactions, or injury. Studies have revealed that cognitive impairments in VD are markedly associated with the modulation of apoptosis and autophagy in neurons of the central nervous system. The concurrent neuronal activation of apoptosis and autophagy hastens neuronal death and cognitive decline [3–5].

Ginkgo Biloba Extract 761 (EGb761), a potent extract derived from the leaves of *G. biloba*, is a globally recognized herbal remedy. It is one of the most clinically scrutinized traditional medicines used for the prevention and treatment of dementia and its associated disorders. EGb761 exhibits a plethora of pharmacological actions, including anti-inflammatory effects, inhibition of lipid peroxidation, scavenging of oxygen-free radicals, enhancement of cerebral blood supply, and regulation of glucose and lipid metabolism, with commendable safety and tolerability [6, 7]. The potential neuroprotective effects of EGb761 in VD, its capacity to enhance learning

and memory in patients with VD, and its role in modulating apoptosis and autophagy in neuronal cells remain unclear.

Given the current research landscape, we selected Sprague–Dawley (SD) rats and used the bilateral common carotid artery occlusion (BCCAO) method to mimic the effects of CCH, thereby establishing a VD rat model. After the procedure, intraperitoneal injections of the standardized Ginkgo biloba extract (EGb761) were administered to monitor changes in cognitive function, morphological alterations in hippocampal neurons, and the possible involvement in the expression of proteins associated with apoptosis and autophagy. Building on this groundwork, the study delved into whether the neuroprotective benefits of EGb761 are interconnected with the activation of the Wnt/ $\beta$ -catenin signaling pathway, aiming to offer a more robust theoretical foundation for EGb761's mechanisms in ameliorating memory and cognitive impairments.

## Methods

### Experimental animals

A total of 40 clean-grade, 3-month-old healthy male Sprague–Dawley (SD) rats, weighing 200–250 g, were purchased from the Experimental Animal Center of Hebei Medical University (certification number: 1709195). After purchasing, the rats were routinely bred in the Clinical Research Center Animal Laboratory of Hebei Province People's Hospital, with the laboratory temperature maintained at 22–24 °C and a humidity of 40–60%. The rats underwent a pre-operative acclimation period of 1 week with free access to food and water. Food was withheld 12 h prior to surgery and water 4 h prior.

### Animal grouping and treatment

The 40 rats were randomly divided into 5 groups, with 8 rats in each group. The sham surgery group (sham group) and the model group (Model group) received intraperitoneal injections of distilled water in the same volume as the other treatment groups, once daily, for a continuous 4 weeks starting the day after surgery. Ginkgo Biloba Extract low-dose group (EGb761-L group): starting the day after surgery, the rats received intraperitoneal injections of EGb761 (Extracted from Ginkgo biloba leaves, from Ginaton®, a standardized preparation) at 25 mg/kg once daily, for a continuous 4 weeks. Ginkgo Biloba Extract high-dose group (EGb761-H group): starting the day after surgery, the rats received intraperitoneal injections of EGb761 at 50 mg/kg once daily, for a continuous 4 weeks. Dickkopf WNT Signaling Pathway Inhibitor1 (DKK1) is a selective inhibitor of the Wnt/ $\beta$ -catenin pathway. To verify whether EGb761 functions through the Wnt/ $\beta$ -catenin signaling pathway, an EGb761

+DKK1 group was added in the experiment. EGb761 +DKK1 group: DKK1 protein dissolved in sterile PBS at a concentration of 1  $\mu\text{g}/\mu\text{l}$ , with a dosing volume of 10  $\mu\text{g}$  for each rat. On the first and fourth day after surgery, 10  $\mu\text{l}$  of the DKK1 solution was injected into the same side lateral ventricle of the rats using a micro-injector.

In this experiment, SD rats were subjected to bilateral common carotid artery occlusion (BCCAO) method, also known as the two-vessel occlusion (2 VO) method, to create a VD rat model. Before the surgery, surgical instruments were steam sterilized for 30 min. The rats were weighed, and an amount of 2% sodium pentobarbital solution calculated at 50 mg/kg was prepared and administered by intraperitoneal injection. Once anesthetized sufficiently, rats were placed in the supine position on the operating table. Carefully cutting the neck fur with scissors, routine iodophor disinfection was performed. A midline neck incision was made, approximately 1.5 cm in length, by longitudinally cutting through the skin, subsequent subcutaneous tissue, and superficial fascia. Blunt separation of the interspace between the sternocleidomastoid, omohyoid, and sternohyoid muscles was performed with small forceps to expose both sides of the common carotid artery sheath, and they were carefully isolated. Care was taken to avoid damaging the thyroid gland. Glass micro needles were used to gently and carefully separate the common carotid artery from the vagus nerve to avoid stretching, clamping, or damaging the vagus nerve. The common carotid arteries of the rats in the model group, EGb761-L group, and EGb761-H group were double ligated with 4-0 surgical sutures to ensure the occlusion of blood flow. Subsequently, the normal anatomical layers of the neck tissue were restored, and the skin was sutured with 0-size surgical sutures. The skin wound was closed, followed by another iodophor disinfection. For the sham surgery group, only careful separation of the bilateral common carotid arteries was performed, slipping two 4-0 surgical sutures around them, without ligating the arteries. Vital signs of the rats were closely monitored during the surgery. After the operation, the rats were placed in lateral decubitus position on dry padding with a covering of padding, and were warmed by incandescent lamps to maintain a rectal temperature of approximately 37 °C until they regained consciousness before returning to the cage. Normal feeding was continued with an ample supply of feed and water.

#### **Morris water maze test**

Ten rats from each group were randomly selected for behavioral experiments, which started at 10:00 each day according to the ID sequence of the rats. The water maze was placed in a room with soft lighting and quiet surroundings. The water maze used in the experiment was

a black cylindrical pool (160 cm in diameter, 60 cm high, 45 cm water depth) with the pool divided evenly into four quadrants. A black circular platform with a diameter of 9 cm was placed in the center of quadrant III at a height of 2 cm below the water surface. Above the water maze, a camera system was fixed at the center of the support, about 2.1 m from the floor, for tracking and recording the swimming tracks of the rats. During the test, the water temperature was maintained at  $25 \pm 1$  °C by an automatic temperature control system [8].

Each day, rats were introduced into the water from the midpoint of the pool wall in one of the three quadrants other than the quadrant containing the platform. Each quadrant was trained at least once daily, with 4 trainings per day, and at least a 30-min interval between each training. Training lasted for 5 days, with the first day starting at quadrants I, IV, II, and I in that order, the second day following the order of IV, II, I, IV, and so on for 5 days to allow all groups of rats to form a memory of the spatial location of the target platform. When placing the rats, they were gently inverted and released into the water facing the pool wall by holding the middle of their tails, allowing them to swim and find the submerged platform. If the rats stayed on the platform for 10 s, it was deemed a successful platform finding. An important point was that each training session was operated by the same person using a consistent technique to minimize human error. The water maze video analysis system automatically tracked and recorded the rat's swimming trajectory and calculated the time it took for the rat to find the hidden underwater platform from entry into the water, recorded as the escape latency; if the rats did not find the hidden platform within 120 s, they were manually guided onto the platform to rest and learn for 10 s, and the escape latency was recorded as 120 s.

On the sixth day of the water maze test, a spatial exploration test was conducted. By removing the platform beforehand and gently introducing rats from the midpoint of the pool wall in the quadrant opposite the original platform (i.e., quadrant I), facing the pool wall, they were allowed to swim freely for 120 s. The water maze video analysis system automatically recorded the time that the rats spent swimming in the platform quadrant (i.e., quadrant III). The percentage of time spent in the target quadrant was calculated as the time spent in the target quadrant divided by 120 s times 100%, serving as an index of the rats' spatial memory ability. This part of the experiment was mainly used to test the spatial memory capabilities of the rats. The experiment should be terminated as soon as the rats become anorexic and depressed during the experiment. In this study, the rats did not develop these conditions. All rats were euthanized using CO<sub>2</sub>. The CO<sub>2</sub> flow rate was 30% container

volume per minute. Anesthetized rats were induced with 4.5% isoflurane gas during euthanasia to reduce anxiety. Euthanasia was determined to be successful 20 min after the rats stopped beating.

#### HE staining

Rat heart tissue was taken, fixed with 4% paraformaldehyde 24 h, gradient ethanol dehydration (70, 80, 95, 100% 1 h each), and embedded in paraffin. 4  $\mu\text{m}$  thick continuous coronal sections were prepared using a slicer (Leica RM2235). After dewaxing and hydration, they were stained with hematoxylin solution (Thermo Fisher) for 3 min, and then differentiated with hydrochloric acid–alcohol differentiation solution. They were blued with saturated disodium hydrogen phosphate solution for 10 min, placed in ethanol, and then stained with eosin for 30 s before baking. The sections were then sealed with neutral gum [9]. The positive control was synchronous staining of the hippocampal tissue of normal rats to verify the effectiveness of the staining system. The negative control was to omit the hematoxylin or eosin staining steps to confirm the non-specific background. Images were collected using the Zeiss Axio Scan.Z1 full slide scanner with a 20  $\times$  objective lens (resolution 0.22  $\mu\text{m}/\text{pixel}$ ) under the same light intensity. The morphological assessment of neuronal injury adopted quantitative analysis: first, the neuronal density. The "Cell Counter" plugin of ImageJ software was used to count the number of pyramidal neurons per  $\text{mm}^2$  in the hippocampal CA1 area; the second was the nuclear shrinkage rate. Five fields of view (200 $\times$ ) were randomly selected to calculate the proportion of neurons with nuclear diameters  $< 5 \mu\text{m}$  and deep staining.

#### Transmission electron microscopy observation

Rat brain tissue was placed on an ice-cold board, with the hippocampus carefully peeled out and a small amount of glutaraldehyde fixative dropped in. Hippocampal CA1 region tissue blocks were cut, trimmed to a size of 1  $\text{mm}^3$ , and immediately fixed in 4% glutaraldehyde for 2–4 h. They were then rinsed three times with 1/15 M phosphate buffer, 15 min each time, followed by fixation in 1% osmium tetroxide for 1–2 h; washed three times with phosphate buffer, 15 min each time, and then dehydrated in a graded series of ethanol (50% ethanol, 70% ethanol, 80% ethanol, 90% ethanol), 15 min each, placed in a 90% ethanol: 90% acetone = 1:1 solution 15 min, 90% acetone 15 min. Finally, they were placed in 100% acetone for 15 min, three times. Infiltration was completed using embedding medium, followed by embedding and shaping the blocks. Ultrathin sections, with a thickness of about 50–70 nm, were cut using an ultramicrotome; stained with uranyl acetate and lead citrate; and observed using

a transmission electron microscope (JEM-1400 PLUS, Japan) to detect mitochondrial morphology.

#### Immunohistochemical staining

Sections were dewaxed and hydrated, antigen remediation: high-pressure thermal remediation with sodium citrate buffer (pH = 6.0) for 15 min, blocked with hydrogen peroxide for endogenous peroxidase at room temperature, protected from light for 10 min. Washed three times with double-distilled water, each time for 5 min. Sections were placed in citrate buffer staining dishes, sealed with a plastic bag, heated to boiling over high heat, and then simmered over low heat for 30 min, washed with PBS three times, 3 min each. Normal goat serum was dropped to block the antigen, incubated at room temperature for 60 min. The primary antibody was added: the serum was discarded, and the serum was dabbed away with filter paper, then 50  $\mu\text{l}$  of appropriately diluted antibody (cleaved caspase-3 1:500, LC3-II 1:300) was dropped. Incubated overnight in a refrigerator at 4  $^{\circ}\text{C}$ . The biotinylated secondary antibody: the next day, after washing three times with PBS, each time for 3 min, biotin-tagged goat anti-rabbit Ig G polymer (Vector Labs, Cat# BA-1000, 1:200) was applied, incubated at room temperature for 60 min, followed by PBS washing three times, 3 min each. DAB (Sigma, Cat# D3939) was used for color development, and it was thoroughly washed with running water. Sections were re-stained with hematoxylin. Dehydrated in graded ethanol, cleared in xylene, and sealed. Finally, the sections were fixed with neutral gum, and after the glue dried, the changes in cell morphology in the hippocampal CA1 region of the rats were observed under the microscope. PBS was used instead of the primary antibody as the negative control to exclude the non-specific binding of the secondary antibody. Images were collected using the Zeiss Axio Scan.Z1 full slide scanner with a 20  $\times$  objective lens (resolution 0.22  $\mu\text{m}/\text{pixel}$ ) under the same light intensity. ImageJ was used to analyze images, set a threshold (background signal + 2  $\times$  SD), segment the positive Area, measure the integrated optical density (IOD) and Area (Area), and calculate the ratio of IOD/Area.

#### Immunofluorescence staining

Cells were fixed with 4% paraformaldehyde for 30 min, washed three times with PBS, blocked with 5% bovine serum albumin for 1 h, and then incubated with the primary antibody (IRGM) at 4 $^{\circ}\text{C}$  overnight. After washing, the fluorescein-conjugated goat anti-rabbit secondary antibody IgG was added and incubated in the dark for 2 h. Fluorescence microscope after DAPI re-staining and sealing (VS200; (Olympus, Japan) Observe, Image J analyzed the stained area, defined the ROI, measured the

average gray value, and subtracted the background (non-stained area).

### Cell culture

The hippocampal neuronal cell line HT22 was purchased from Wuhan Puno Sai Life Technology Co., Ltd. HT22 cells were cultured in low-glucose, low-serum medium under 1% O<sub>2</sub>, and in normal glucose, normal serum medium under 95% air. Then, HT22 cells cultured in a low-oxygen environment were treated with EGb761, H<sub>2</sub>O<sub>2</sub>, and DKK1. Cells were divided into sham group, Model group, EGb761 group, EGb761 + H<sub>2</sub>O<sub>2</sub> group, and EGb761 + DKK1 group.

### Western blotting

Cells or tissues were digested with trypsin and rinsed with PBS, lysed with RIPA lysis buffer to prepare total cell protein. The protein concentration was measured by the BCA method. Samples were mixed with loading buffer and boiled in a metal bath for 10 min. Proteins (20 µg/lane) were electrophoresed on polyacrylamide gels and then transferred to PVDF membranes. The membranes were blocked with 5% skim milk at room temperature for 2 h, then incubated with the primary antibody overnight at 4 °C. The next day, after washing the membrane with TBST, the HRP-conjugated secondary antibody was incubated at room temperature for 2 h. After washing with TBST, an appropriate amount of ECL chemiluminescent solution was dropped. Exposed in the gel imaging system and the grayscale value was analyzed. Image Lab 6.0 (Bio-Rad) was used to analyze the gray values of the bands. With GAPDH as the internal reference, the relative expression level of the target protein (target protein/internal reference) was calculated.

### Statistical analysis

Data and graphics were analyzed using Prism 9.0 software. The Shapiro–Wilk method was used for normality tests. The univariate ANOVA or Kruskal–Wallis test (for non-parametric data) was used for inter-group comparisons. The Tukey method or Dunn method was used for post hoc tests. Multiple comparisons were corrected by Bonferroni. The data were expressed as mean ± standard deviation ( $\bar{x} \pm s$ ), with \* $P < 0.05$  and \*\* $P < 0.01$  being considered significant differences. If the data did not meet the basic requirements, they were directly discarded.

## Results

### Effects of EGb761 on behavioral and spatial learning abilities of rats

After excluding rats that died post-surgery, suffered serious infections, had low body weight, hemiplegia, or visual system damages, the number of experimental rats

was supplemented, resulting in a total of 40 rats undergoing the water maze experiment, with 10 in each group. Rats were treated with EGb761 continuously for 4 weeks after BCCAO surgery. On the second day after discontinuing the drug, all rats underwent place navigation tests. The data showed statistically significant differences in the average escape latency between the four groups. Upon further pairwise comparison between groups, on the first day of the test, the escape latency of the rats in both the high-dose and low-dose EGb761 groups showed no statistical difference from the Model group, suggesting no difference between the two groups. However, the average escape latency of the Model group was longer than that of the sham-operated group, which was significantly prolonged from the second to the fifth day after surgery, indicating a successful VD (vascular dementia) rat model. From the second to the fifth day of training, the escape latency of rats in both the high- and low-dose groups of EGb761 was significantly reduced compared to the Model group, with statistically significant differences between the groups. From the third to the fifth day, the decrease in escape latency was more pronounced in the high-dose EGb761 group compared to the low-dose group, with a statistically significant difference.

The results of the spatial exploration test indicated statistically significant differences in the percentage of time spent in the target quadrant among the four groups of rats. Compared to the sham-operated group, the percentage of time the rats in the Model group and the low-dose EGb761 group spent in the target quadrant was significantly reduced ( $P < 0.01$ ). Compared to the Model group, the percentage of time spent in the target quadrant by rats in the high-dose EGb761 group was significantly increased, with no statistical difference from the low-dose EGb761 group ( $P < 0.01$ ). The difference in the percentage of time rats spent in the target quadrant between the high-dose and low-dose EGb761 groups was statistically significant. The swimming trajectories of the rats are shown in the figure, with the sham-operated group's trajectories gradually approaching a straight line, indicating a significant reduction in time taken. In contrast, most Model group rats continued to swim along the edges, indicating an apparent memory impairment in learning compared to the other groups, with both the sham-operated and treated groups outperforming the Model group in learning and memory ability (Fig. 1A).

### Effects of EGb761 on the pathological changes of rats with vascular dementia

Hematoxylin and eosin (HE) staining results showed that the arrangement of pyramidal neurons in the CA1 area of the hippocampus in the Sham group was neat and dense, with mostly intact cell structures, full

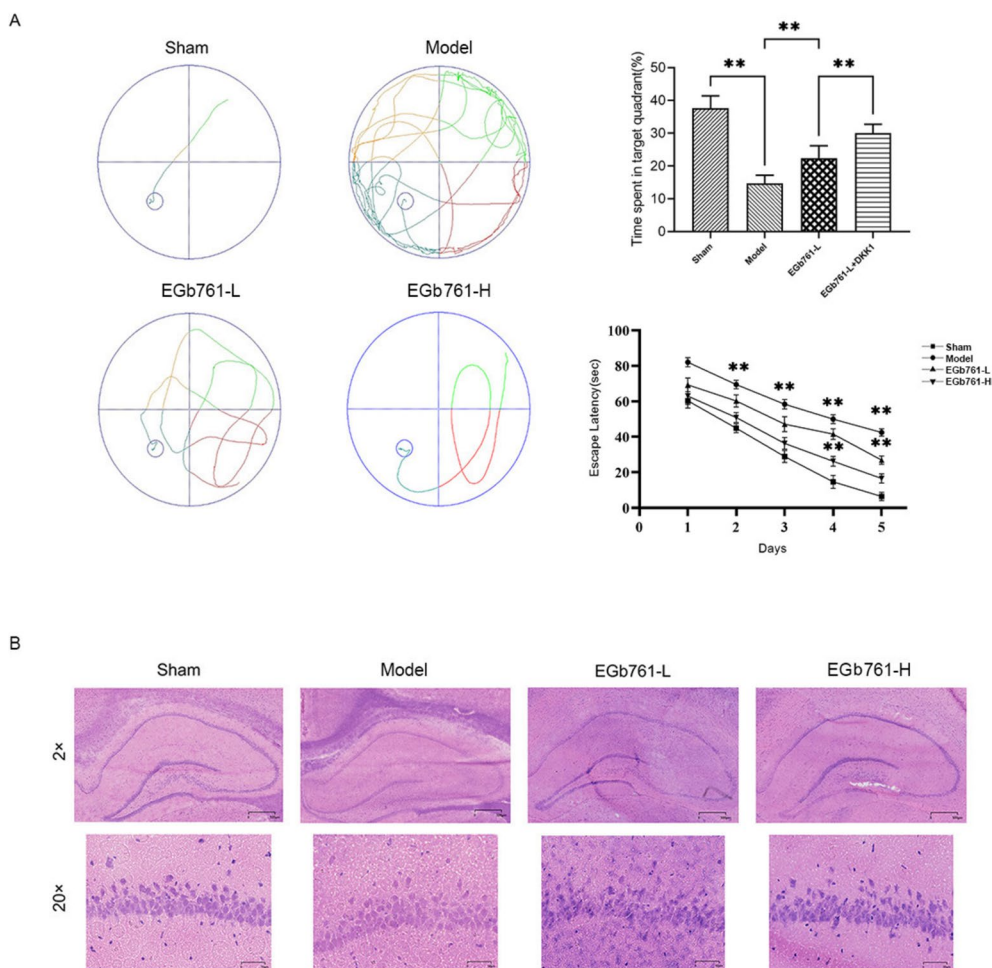


**Fig. 1** EGb761 can improve behavioral and spatial learning abilities and brain injury in rats with vascular dementia. **A** Changes in the escape latency of four groups of rats, the percentage of time spent in the target quadrant, and swimming trajectories during the spatial exploration test after the platform was removed; **B** HE staining observation of morphological changes in the hippocampal CA1 region of rats in each group; **C** transmission electron microscopy images of hippocampal CA1 region neurons of rats in the four groups. Data are expressed as mean ± standard deviation. *N* = 8, *P* < 0.05 is considered statistically significant. <sup>n</sup>*S* *P* > 0.05; \**P* < 0.05; \*\**P* < 0.01

shapes, and clearly visible nucleoli, without significant neuron loss. In contrast, the Model group displayed evident loss and decreased numbers of pyramidal neurons, with a more disorganized arrangement, partial cells becoming spindle-shaped or irregular, condensed nuclei with deep staining, and pale cytoplasm, with some nucleoli becoming obscured. The high-dose EGb761 group had less neuronal damage than the Model group, with fewer lost cells, a relatively dense cellular arrangement, relatively intact cell structures, and fewer incidences of nuclear condensation and deep staining than the Model group. The low-dose EGb761 group exhibited a minor neuron loss compared to the high-dose group, with a slightly more scattered arrangement and relatively intact cell structures, though some cell bodies were deformed or nuclei condensed. Electron microscopy observations showed

that the Sham group had clear nuclear membranes, normal chromatin structure, and complete ultrastructure of various organelles, with only a few autophagic bodies in some neurons. However, the Model group exhibited many autophagic bodies, severe mitochondrial swelling, disappearance of mitochondrial cristae, endoplasmic reticulum expansion, partial dissolution of the nuclear membrane, and only unclear boundaries in some cells. In the low-dose EGb761 group, there was mitochondrial swelling, endoplasmic reticulum expansion, and fewer autophagic bodies than in the Model group, with irregular nuclear membrane changes. The high-dose EGb761 group also showed some mitochondrial swelling, lighter than in the low-dose group, fewer autophagic bodies than in the Model group, with normally shaped lysosomes, endoplasmic reticulum, and nuclear membrane (Fig. 1B, C).

**Effects of EGb761 on apoptosis and autophagy-related proteins in rats with vascular dementia**

Immunohistochemical staining results showed a marked increase in cleaved caspase-3 positive cells in the CA1 area of the hippocampus in the Model group compared to the sham-operated group ( $P < 0.01$ ). Both the high and low doses of EGb761 groups showed significant reductions in cleaved caspase-3 positive cells compared to the Model group, with lower levels in the high-dose group ( $P < 0.01$ ).

In terms of LC3-II, the Model group showed a significant increase compared to the sham-operated group ( $P < 0.01$ ), while both the high and low-dose EGb761 groups had reduced LC3-II positive expressions compared to the Model group. However, this reduction was more significant in the high-dose group, showing a statistical difference ( $P < 0.01$ ) (Fig. 2).

**EGb761 mediates the Wnt/ $\beta$ -catenin signaling pathway to inhibit brain injury in rats with vascular dementia**

HE staining showed that the CA1 area of the hippocampus in the sham-operated group had many neurons with an orderly arrangement and no significant neuron loss; the cells were regularly shaped with complete structures, full nuclei, and clear nucleoli. The Model

group had fewer neurons in the hippocampal CA1 area; there was significant loss and a more scattered arrangement, irregular shaped cytoplasm, shrunken and deeply stained nuclei, disappearing nucleoli, and pale cytoplasm. The EGb761 group had less neuronal damage in the hippocampal CA1 area than the Model group, with fewer neuron losses, relatively dense and ordered arrangements, relatively intact cell structures, no significant shrinkage, and reduced nuclear condensation and deep staining compared to the Model group. The EGb761 + DKK1 group revealed partial neuron loss, a somewhat scattered arrangement, and observable changes, such as cell body deformation, shrunken cells, and deeply stained nuclei.

Immunofluorescence staining results showed that the Model group's relative fluorescence intensity of IRGM was significantly higher compared to the sham-operated group ( $P < 0.01$ ), while the EGb761 group showed a significant reduction compared to the Model group ( $P < 0.01$ ). When compared to the EGb761 group, the EGb761 + DKK1 group had a markedly increased IRGM relative fluorescence intensity ( $P < 0.01$ ), indicating that EGb761 can mediate the Wnt/ $\beta$ -catenin signaling pathway to inhibit apoptosis in hippocampal neurons in VD rats (Fig. 3).

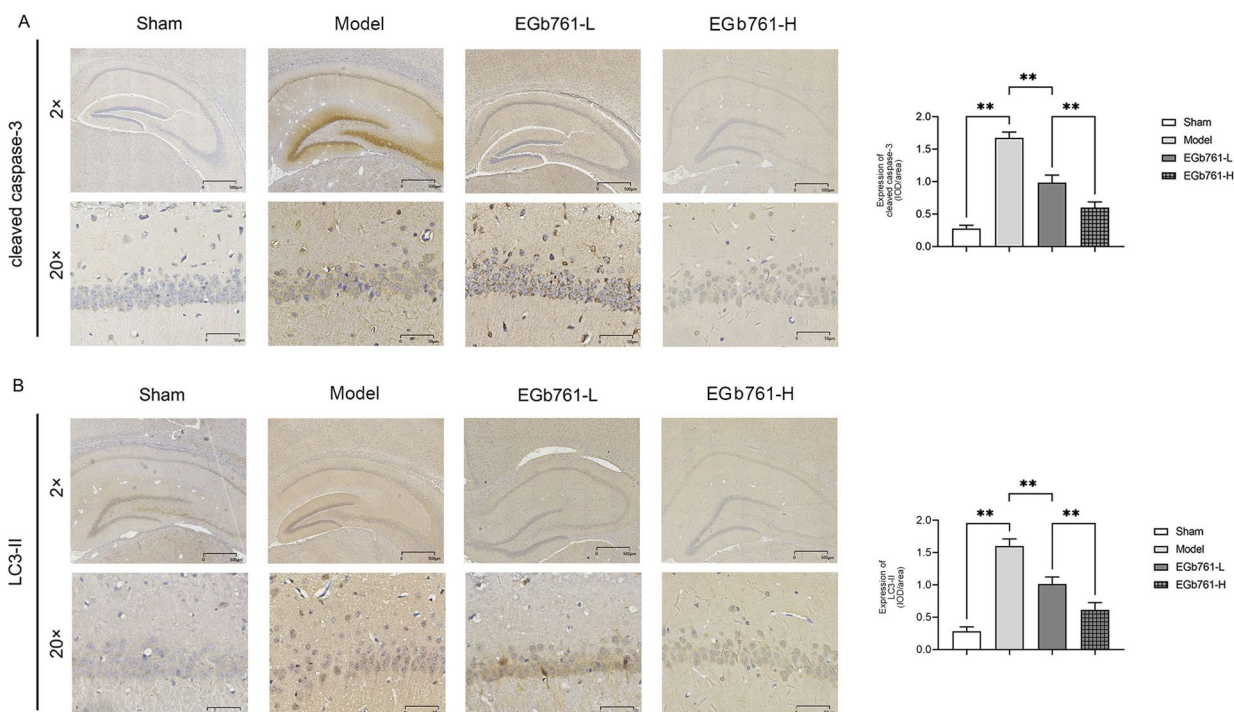


**Fig. 2** EGb761 inhibits the expression of apoptosis and autophagy-related proteins in rats with vascular dementia. **A** Immuno-positive cell expression of cleaved caspase-3 in the hippocampal CA1 region of four groups of rats and statistical results of IOD/area values; **B** immuno-positive cell expression of LC3-II in the hippocampal CA1 region of four groups of rats and statistical results of IOD/area values. Data are expressed as mean  $\pm$  standard deviation.  $N = 8$ ,  $P < 0.05$  is considered statistically significant.  $^{ns}P > 0.05$ ;  $^{*}P < 0.05$ ;  $^{**}P < 0.01$

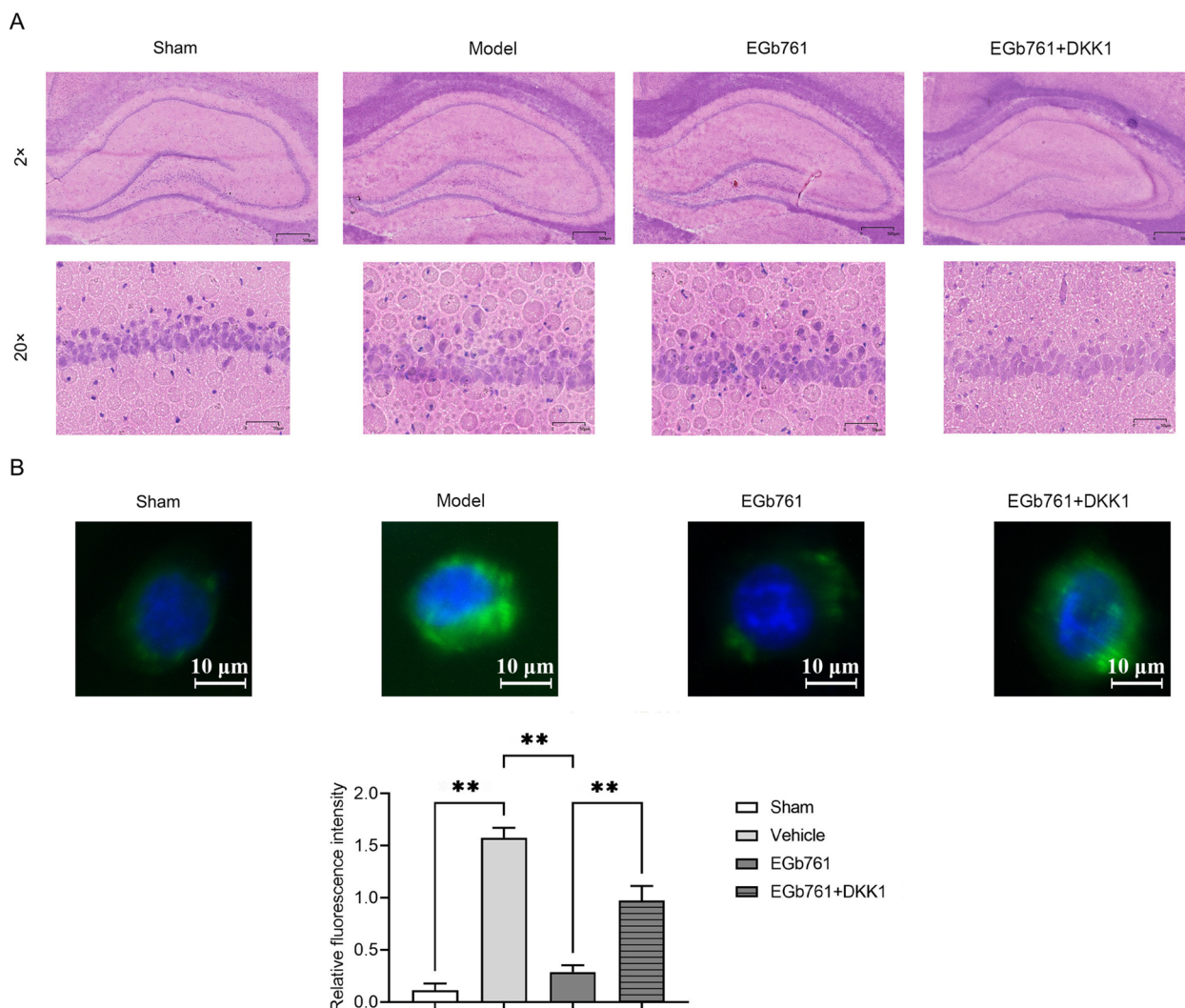


**Fig. 3** EGb761 can activate the Wnt/ $\beta$ -catenin signaling pathway to inhibit brain damage in rats with vascular dementia. **A** HE staining observation of morphological changes in the hippocampal CA1 region of rats in each group; **B** immunofluorescence staining images of IRGM in the hippocampal CA1 region of four groups of rats and statistical results of relative fluorescence intensity. Data are expressed as mean  $\pm$  standard deviation.  $N = 3$ ,  $P < 0.05$  is considered statistically significant.  $^{ns}P > 0.05$ ;  $^{*}P < 0.05$ ;  $^{**}P < 0.01$

**EGb761 inhibits apoptosis of hippocampal neurons through the suppression of ROS signaling pathways**

Western blotting results indicated that relative protein expression levels of P22, P47, p-JNK, p-c-JUN, P53, and IRGM in the Model group increased significantly compared to the sham group. In the EGb761 group, these levels were significantly lower in contrast to the Model group. However, relative protein expression levels of P22, P47, p-JNK, p-c-JUN, P53, and IRGM increased significantly in the EGb761 + H<sub>2</sub>O<sub>2</sub> group compared to the EGb761 group.

Immunofluorescence staining experiments revealed that compared to the sham group, the Model group’s relative fluorescence intensity of IRGM was significantly

higher ( $P < 0.01$ ), whereas the EGb761 group showed significant reductions compared to the Model group ( $P < 0.01$ ). The EGb761 + H<sub>2</sub>O<sub>2</sub> group had a markedly increased IRGM relative fluorescence intensity in comparison with the EGb761 group ( $P < 0.01$ ), suggesting that EGb761 can inhibit apoptosis of hippocampal neurons through the suppression of ROS signaling pathways (Fig. 4).

**EGb761 mediates the Wnt/ $\beta$ -catenin signaling pathway to inhibit apoptosis and autophagy in hippocampal neurons**

Western blotting results showed that relative protein expression levels of  $\beta$ -catenin, P53, IRGM, TFEB, LC3,

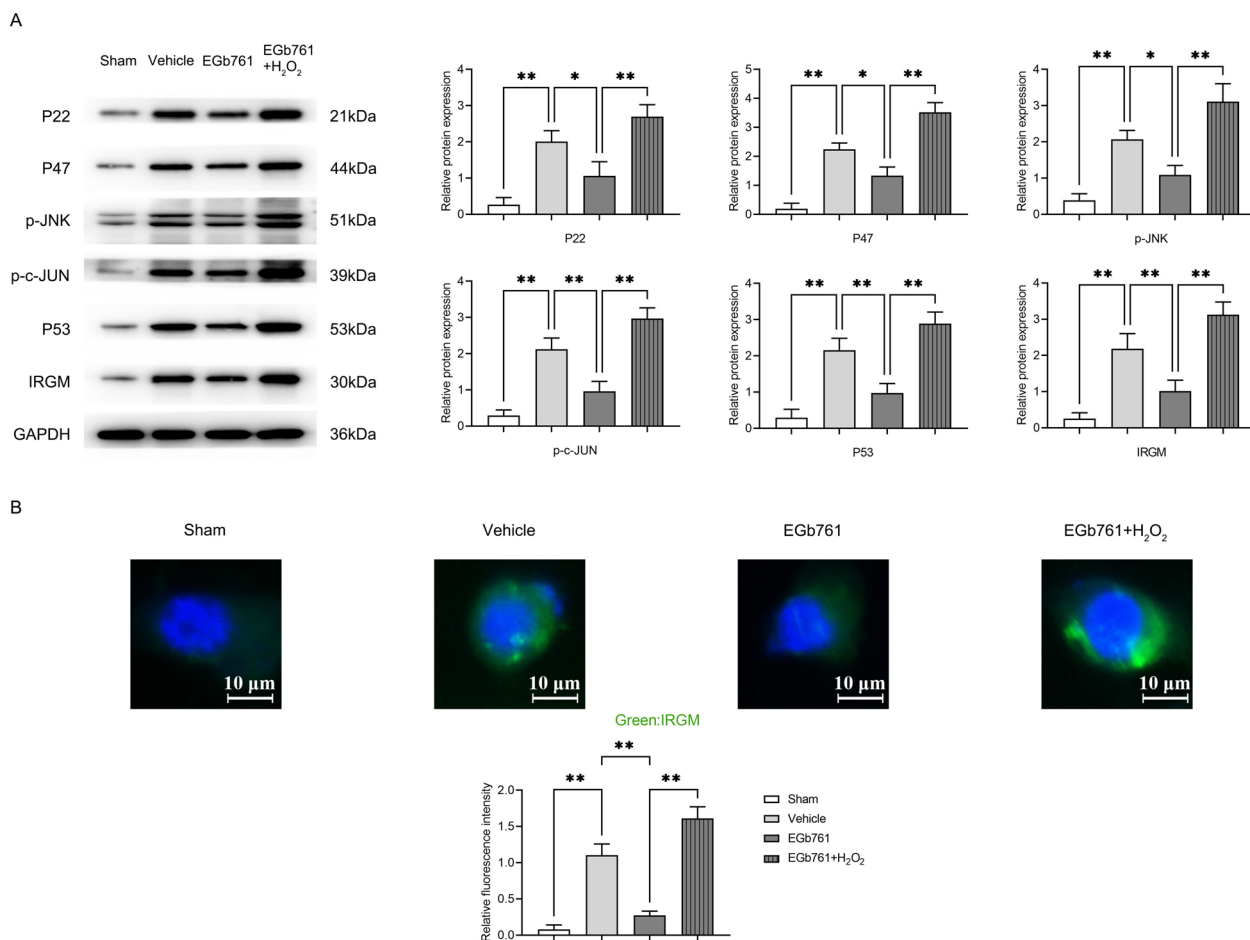


**Fig. 4** EGb761 can inhibit apoptosis of hippocampal neurons through the ROS signaling pathway. **A** Protein band images of P22, P47, p-JNK, p-c-JUN, P53, and IRGM, and statistical results of relative protein expression levels; **B** immunofluorescence staining images of IRGM and P53 and statistical results of relative fluorescence intensity. Data are expressed as mean ± standard deviation. *N* = 3, *P* < 0.05 is considered statistically significant. <sup>ns</sup>*P* > 0.05; \**P* < 0.05; \*\**P* < 0.01

LAMP1, and SQSTM1 in the Model group were significantly higher compared to the sham group. The EGb761 group demonstrated significant reductions in these relative protein expressions compared to the Model group, while the EGb761 + DKK1 group showed significantly higher levels than the EGb761 group.

Transmission electron microscopy observations indicated that the Sham group had clear nuclear membranes, intact ultra-structures of various organelles, and only a few autophagic bodies seen in neurons. More autophagic bodies, severe mitochondrial swelling, disappearance of mitochondrial cristae, endoplasmic reticulum expansion, and partial dissolution of nuclear membranes with unclear borders were noted in the Model group. The EGb761 group showed slight mitochondrial swelling with reduced autophagic bodies and normally shaped lysosomes, endoplasmic reticulum,

and nuclear membrane, whereas the EGb761 + DKK1 group exhibited swollen mitochondria, expanded endoplasmic reticulum, decreased autophagic bodies, and irregular nuclear membrane changes (Fig. 5). Compared with the EGb761 group, the addition of DKK1 significantly reversed the inhibitory effect of EGb761 on apoptosis and autophagy-related proteins, and simultaneously weakened its improvement effect on neuronal injury. This result reverse confirms that the neuroprotective effect of EGb761 needs to be achieved by activating the Wnt/β-catenin signaling pathway.

These results indicated that EGb761 mediates the Wnt/β-catenin signaling pathway to inhibit apoptosis and autophagy in hippocampal neurons of VD rats, improving damage in vascular dementia rats (Fig. 6).

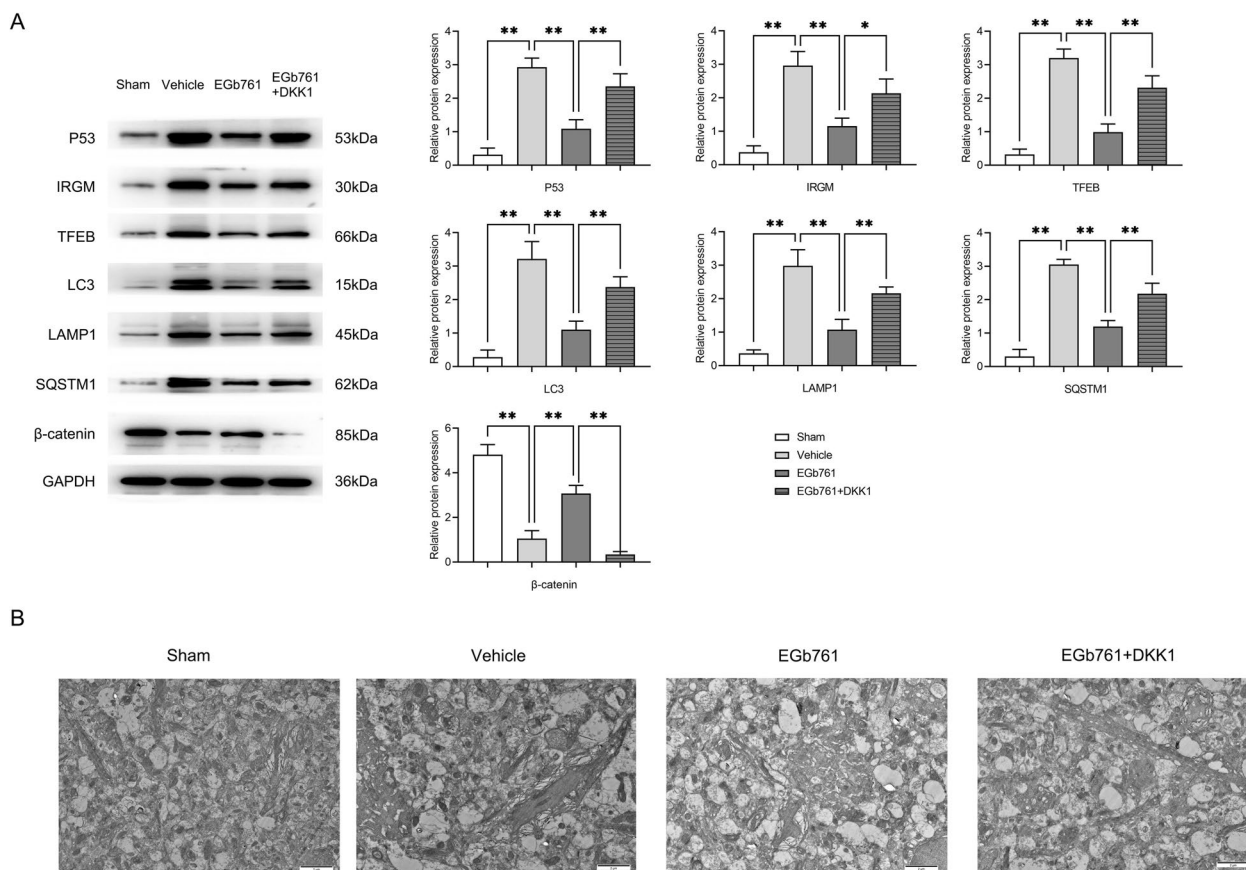


**Fig. 5** EGb761 can mediate the Wnt/ $\beta$ -catenin signaling pathway to inhibit apoptosis and autophagy of hippocampal neurons. **A** Protein band images of  $\beta$ -catenin, P53, IRGM, TFEB, LC3, LAMP1, and SQSTM1, and statistical results of relative protein expression levels; **B** transmission electron microscopy images of hippocampal neurons. Data are expressed as mean  $\pm$  standard deviation.  $N = 3$ ,  $P < 0.05$  is considered statistically significant. <sup>ns</sup> $P > 0.05$ ; \* $P < 0.05$ ; \*\* $P < 0.01$

### Discussion

Vascular dementia (VD) is a heterogeneous cerebrovascular condition in which cognitive decline can be traced to the cerebrovascular pathology. It is the second most prevalent type of dementia, accounting for over 20% of dementia cases, surpassed only by Alzheimer’s disease (AD). The demographic shift towards an aging population and the rising incidence of stroke have contributed to an escalating prevalence of VD. Vascular cognitive impairment and dementia have emerged as increasingly prevalent ailments among older adults, imposing a formidable burden on society and families [10–13]. A complete understanding of the pathogenesis of VD remains elusive, a shortcoming that has given rise to the absence of efficacious targeted therapeutic agents, a critical concern that has garnered the attention of the medical community.

The hippocampus, a vital region intricately connected to spatial learning and long-term memory, has recently become a focal point in neuroscientific research [14, 15]. Injury or necrosis of neuronal cells during hippocampal

formation results in cognitive deficits. VD rats treated with EGb761 demonstrated a marked reduction in escape latency during the Morris water maze test compared with the model group, along with a substantial increase in the time spent in the target quadrant during the spatial exploration test. This indicated that EGb761 treatment markedly enhanced spatial learning and memory capabilities in VD rats, thereby validating its therapeutic efficacy. Histological examination via HE staining revealed that EGb761 mitigated neuronal cell loss, promoting a more densely packed and orderly cellular arrangement with preserved cellular structures and no notable reduction in cell size or nuclear pyknosis. Transmission electron microscopy further confirmed that EGb761 ameliorated the condition of damaged hippocampal neurons in VD rats, thereby reducing the incidence of autophagy.

Apoptosis, a form of programmed cell death characterized by an orderly and active process, is the physiological and pathological mechanism that orchestrates cell death and facilitates cell clearance. Previous studies

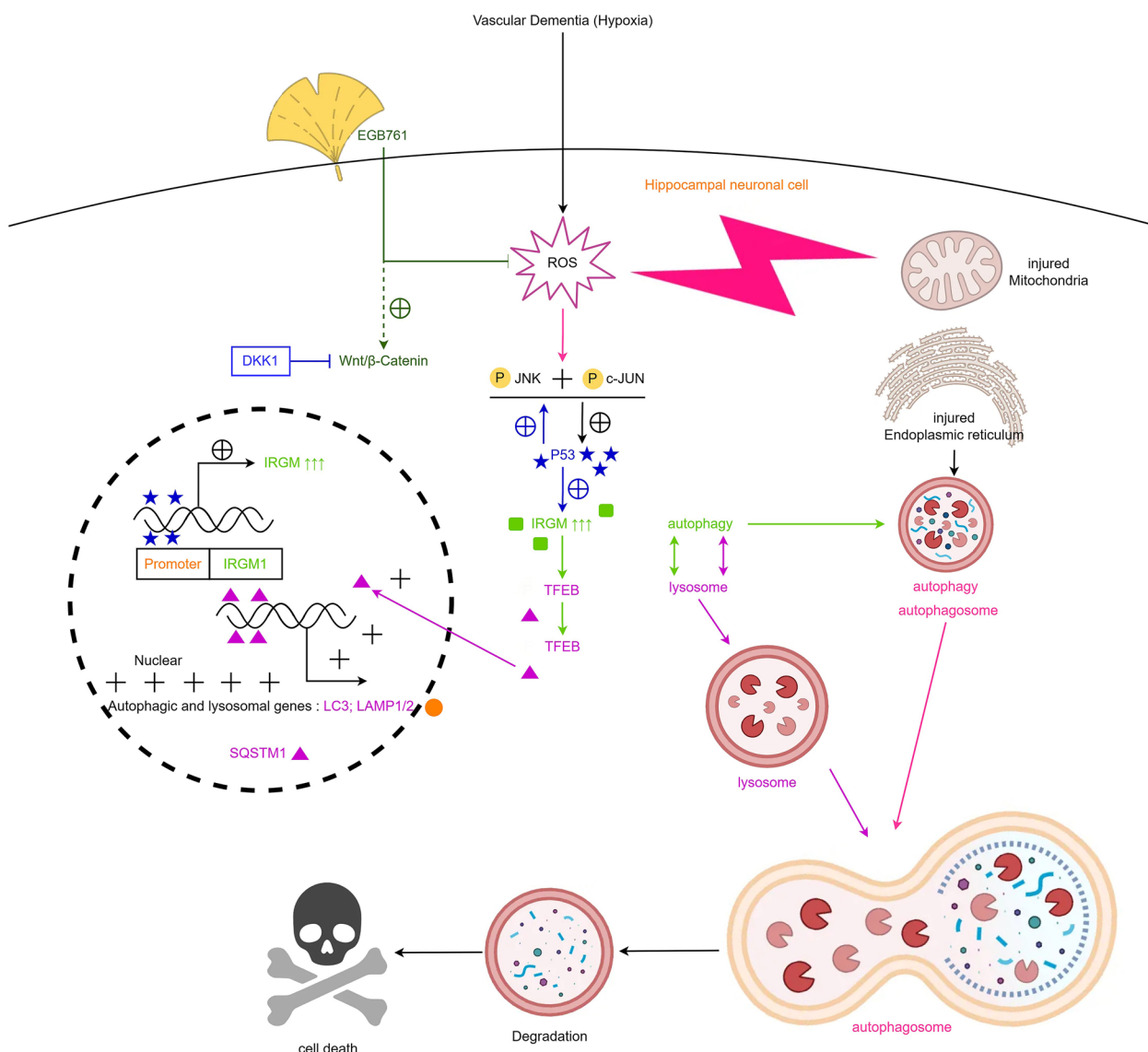


**Fig. 6** EGb761 mediates the Wnt/β-catenin signaling pathway to inhibit apoptosis and autophagy of hippocampal neuronal cells in rats with vascular dementia, thereby improving the damage in rats with vascular dementia

have demonstrated that Bcl-2 exerts an inhibitory effect on apoptosis; increased expression of Bcl-2 is associated with enhanced cell survival, whereas Bax, a pro-apoptotic protein, promotes apoptosis, with higher expression levels resulting in greater cell death [16–18]. In addition, cleaved caspase-3 and P53 are pivotal factors in apoptosis that synergistically lead to cell death. These results indicate that EGb761 dose-dependently inhibited apoptosis in the hippocampal neurons of VD rats, exerting a more pronounced anti-apoptotic effect at higher doses, thus fulfilling a neuroprotective role.

Autophagic cell death, a subset of programmed cell death, coexists with apoptosis and engages in an intricate

interplay. Autophagy functions as a self-protective mechanism for neurons, clearing aberrant accumulation and sustaining cellular viability. However, ischemic injury can trigger excessive autophagy, culminating in cell death [19, 20]. P62, also known as SQSTM1, participates in diverse signaling pathways and is ubiquitously expressed in various cells and tissues. It serves as a bridge between LC3 and the ubiquitinated substrates, facilitating their integration into the autophagosome. When autophagy is activated, autophagosomes merge with lysosomes, leading to the lysosomal degradation of p62, thereby reducing its expression levels. Conversely, inhibition of autophagy results in elevated p62 levels [21, 22]. Beclin

1, a fundamental molecule in autophagosome formation, plays a critical role in regulating the generation and expansion of autophagosomes, and its expression levels increase during autophagy. LC3, a key constituent of the autophagosomal membrane, exists in two interchangeable forms, LC3-I and LC3-II. LC3-II is widely recognized as a molecular marker of autophagy, with its abundance reflecting the degree of autophagic activity [23, 24]. Lysosome-associated membrane protein (LAMP) family proteins, such as LAMP-1 and LAMP-2, are essential for maintaining lysosomal integrity and the acidic milieu, as well as facilitating the fusion of lysosomes with autophagosomes [25, 26].

In the present study, EGb761 treatment decreased the expression of LC3-II and Beclin1 in the hippocampal neurons of VD rats while augmenting the expression of p62 protein. This substantiates the idea that EGb761 curtails the excessive activation of autophagy in hippocampal neurons, thereby safeguarding these neurons and ameliorating cognitive impairment, thus reinforcing its neuroprotective potential.

Oxidative stress is a critical factor in the pathogenesis of vascular dementia, and is characterized by an imbalance between reactive oxygen species (ROS) and antioxidant defense mechanisms within cells, resulting in the accumulation of oxidative compounds and subsequent cellular damage. In the context of vascular dementia, diminished cerebral blood flow can induce cellular hypoxia and reperfusion injury, often accompanied by ROS overproduction [27, 28]. In cellular stress responses, ROS function as signaling molecules that activate the JNK pathway. On one hand, the generation can precipitate the oxidation of cellular proteins and lipids, triggering c-Jun N-terminal kinase (JNK) activation, which in turn phosphorylates c-Jun and modulates the expression of stress-responsive genes [29, 30]. JNK (c-Jun N-terminal kinase) and the Wnt/ $\beta$ -catenin signaling pathways are two paramount cell signaling cascades. The Wnt/ $\beta$ -catenin pathway is a highly conserved mechanism vital for normal embryonic development and adult tissue homeostasis. Studies have illustrated that JNK activation can inhibit Wnt/ $\beta$ -catenin signaling by phosphorylating components of the Wnt pathway, such as Dishevelled (Dvl), and by inducing  $\beta$ -catenin degradation, thereby reducing nuclear  $\beta$ -catenin accumulation and the expression of Wnt target genes. Moreover, Wnt/ $\beta$ -catenin signaling can downregulate P53 expression, while JNK can upregulate P53 [31, 32]. Research has elucidated that P53 is implicated in the regulation of IRGM expression and P53 stability through interactions with the ribosomal protein L11 (RPL11) and transformed mouse 3T3 MDM2 cells. IRGM modulates autophagy to combat intracellular pathogenic infections and clear cellular damage. IRGM

functions as a regulatory factor in the host autophagic response, particularly against intracellular pathogens, such as bacteria and viruses. Upon infection with these pathogens, IRGM facilitates the formation of autophagosomes that encapsulate and isolate the pathogens, which are then degraded and eliminated via lysosomal fusion. TFEB, a member of the MiT/TFE family of transcription factors, which includes TFEB, TFE3, MITF, and TFEC, is the principal regulator of lysosomal biogenesis and autophagy. It modulates the expression of genes involved in these processes by binding to the Coordinated Lysosomal Expression and Regulation (CLEAR) sequences in their promoters. Studies have shown that IRGM promotes autophagosome assembly and maturation around intracellular pathogens. By coordinating the actions of IRGM and TFEB, cells can efficiently localize and eliminate pathogens or damaged organelles through lysosomal degradation [33, 34].

In this study, we found that EGb761 can inhibit the expression of P22, P47, p-JNK, p-c-JUN,  $\beta$ -catenin, TFEB, LC3, LAMP1, SQSTM1, P53, and IRGM; and after treatment with H<sub>2</sub>O<sub>2</sub> and DKK1, the inhibitory effects of EGb761 on the above proteins were eliminated. Meanwhile, it weakened its improvement effect on neuronal injury. Although this study systematically explored the mechanism by which EGb761 improves vascular dementia (VD) through the Wnt/ $\beta$ -catenin pathway, there are still limitations, such as a single animal model, a small sample size, and no involvement of human samples. These problems will be further improved in subsequent studies.

In summary, EGb761 modulates the Wnt/ $\beta$ -catenin signaling pathway to inhibit both apoptosis and autophagy in hippocampal neurons of rats with vascular dementia, consequently mitigating the detrimental effects of vascular dementia. These findings suggest novel therapeutic targets and methodologies for the treatment of vascular dementia. However, this study must be validated in relevant clinical trials to validate the findings. In this study, we used male rats for the experiments, and subsequent experiments used female rats for further validation of the experimental results.

### Supplementary Information

The online version contains supplementary material available at <https://doi.org/10.1186/s40001-025-02681-6>.

Additional file 1

### Acknowledgements

None.

### Author contributions

N.Y. and Z.P.D., study concept and design. N.Y., manuscript writing, Morris water maze and western blotting. Y.Y.Y. and X.Q.L., directed flow cytometric studies

and cell culture and processing. R.S.D and G.D.X, Immunohistochemical Staining and HE. P.Y.L, data analysis. All authors read and approved the final manuscript.

#### Funding

This study was funded by Hebei Province Medical Science Research Key Project (no. 2019-139-5), Hebei Province Introducing Foreign Intellectual Project (no. 2020-2).

#### Availability of data

The datasets generated during and/or analysed during the current study are available from the corresponding author on reasonable request.

#### Declarations

##### Ethics approval and consent to participate

This study has been reviewed and approved by Medical Ethics Committee of Hebei Provincial People's Hospital (202398).

##### Consent for publication

Not applicable.

##### Competing interest

The authors declare no competing interests.

Received: 22 August 2024 Accepted: 12 May 2025

Published online: 19 June 2025

#### References

- Zhu Y, Liu H, Lu XL, et al. Prevalence of dementia in the People's Republic of China from 1985 to 2015: a systematic review and meta-regression analysis. *BMC Public Health*. 2019;19(1):578.
- Zhu T, Zhu M, Qiu Y, et al. Puerarin alleviates vascular cognitive impairment in vascular dementia rats. *Front Behav Neurosci*. 2021;15: 717008.
- Xu J, Qi Q, Lv P, et al. Oxiracetam ameliorates cognitive deficits in vascular dementia rats by regulating the expression of neuronal apoptosis/autophagy-related genes associated with the activation of the Akt/mTOR signaling pathway. *Br J Med Biol Res Revista brasileira de pesquisas medicas e biologicas*. 2019;52(11):e8371.
- Yan N, Zhang JJ. The emerging roles of Ferroptosis in vascular cognitive impairment. *Front Neurosci*. 2019;13:811.
- Wang XX, Zhang B, Xia R, et al. Inflammation, apoptosis and autophagy as critical players in vascular dementia. *Eur Rev Med Pharmacol Sci*. 2020;24(18):9601–14.
- Wang M, Peng H, Peng Z, et al. Efficacy and safety of ginkgo preparation in patients with vascular dementia: a protocol for systematic review and meta-analysis. *Medicine*. 2020;99(37): e22209.
- García-Alberca JM, Mendoza S, Gris E. Benefits of treatment with ginkgo biloba extract EGb 761 alone or combined with acetylcholinesterase inhibitors in vascular dementia. *Clin Drug Invest*. 2022;42(5):391–402.
- Ning Z, Zhong X, Wu Y, et al.  $\beta$ -asarone improves cognitive impairment and alleviates autophagy in mice with vascular dementia via the cAMP/PKA/CREB pathway. *Phytomed Int J Phytother Phytopharmacol*. 2024;123: 155215.
- Gao Y, Ma K, Zhu Z, et al. Modified Erchen decoction ameliorates cognitive dysfunction in vascular dementia rats via inhibiting JAK2/STAT3 and JNK/BAX signaling pathways. *Phytomed Int J Phytother Phytopharmacol*. 2023;114: 154797.
- Zupanic E, von Euler M, Winblad B, et al. Mortality after ischemic stroke in patients with Alzheimer's disease dementia and other dementia disorders. *J Alzheimer's Dis JAD*. 2021;81(3):1253–61.
- Zuliani G, Trentini A, Rosta V, et al. Increased blood BACE1 activity as a potential common pathogenic factor of vascular dementia and late onset Alzheimer's disease. *Sci Rep*. 2020;10(1):14980.
- Zou H, Chen X, Lu J, et al. Neurotrophin alleviates cognitive impairment by inhibiting TLR4/MyD88/NF- $\kappa$ B inflammation signaling pathway in mice with vascular dementia. *Neurochem Int*. 2023;171: 105625.
- Zuin M, Cherubini A, Volpato S, et al. Acetylcholinesterase-inhibitors slow cognitive decline and decrease overall mortality in older patients with dementia. *Sci Rep*. 2022;12(1):12214.
- Zhu SJ, Li X, Wei YW, et al. Acupoint catgut embedding improves learning and memory impairment in vascular dementia rats. *Ann Transl Med*. 2023;11(2):108.
- Zhang Y, Li Y, Wang Y, et al. Effects of resveratrol on learning and memory in rats with vascular dementia. *Mol Med Rep*. 2019;20(5):4587–93.
- Zhang M, Huang SS, He WY, et al. Nasal administration of bFGF-loaded nanoliposomes attenuates neuronal injury and cognitive deficits in mice with vascular dementia induced by repeated cerebral ischemia-reperfusion. *Int J Nanomed*. 2024;19:1431–50.
- Zhai W, Zhao M, Zhang G, et al. MicroRNA-based diagnosis and therapeutics for vascular cognitive impairment and dementia. *Front Neurol*. 2022;13: 895316.
- Yang K, Zeng L, Ge A, et al. Exploring the oxidative stress mechanism of Buyang Huanwu decoction in intervention of vascular dementia based on systems biology strategy. *Oxid Med Cell Longev*. 2021;2021:8879060.
- Tian A, Ma X, Li H, et al. DI-3n-butylphthalide improves spatial learning and memory in rats with vascular dementia by reducing autophagy via regulation of the mTOR signaling pathway. *Exp Ther Med*. 2020;19(3):1940–6.
- Xu L, Qu C, Liu Y, et al. The environmental enrichment ameliorates chronic cerebral hypoperfusion-induced cognitive impairment by activating autophagy signaling pathway and improving synaptic function in hippocampus. *Brain Res Bull*. 2023;204: 110798.
- Zou YJ, Xu JJ, Wang X, et al. Lactobacillus johnsonii L531 ameliorates *Escherichia coli*-induced cell damage via inhibiting NLRP3 inflammatory activity and promoting ATG5/ATG16L1-mediated autophagy in porcine mammary epithelial cells. *Veterinary Sci*. 2020;7(3).
- Zou B, Liu J, Klionsky DJ, et al. Extracellular SQSTM1 as an inflammatory mediator. *Autophagy*. 2020;16(12):2313–5.
- Zou T, Gao S, Yu Z, et al. Salvianolic acid B inhibits RAW264.7 cell polarization towards the M1 phenotype by inhibiting NF- $\kappa$ B and Akt/mTOR pathway activation. *Sci Rep*. 2022;12(1):13857.
- Zou R, Wu S, Wang Y, et al. Role of integrin-linked kinase in static compressive stress-induced autophagy via phosphatidylinositol 3 kinase in human periodontal ligament cells. *Int J Mole Med*. 2021;48(3).
- Yu Q, Zou L, Yuan X, et al. Dexmedetomidine protects against septic liver injury by enhancing autophagy through activation of the AMPK/SIRT1 signaling pathway. *Front Pharmacol*. 2021;12: 658677.
- Yihao D, Tao G, Zhiyuan W, et al. Ginkgo biloba leaf extract (EGb-761) elicits neuroprotection against cerebral ischemia/reperfusion injury by enhancement of autophagy flux in neurons in the penumbra. *Iran J Basic Med Sci*. 2021;24(8):1138–45.
- Zhu J, Du J, Kou W, et al. Probucol protects against brain damage caused by intra-neural pyroptosis in rats with vascular dementia through inhibition of the Syk/Ros pathway. *Aging*. 2024;16(5):4363–77.
- Wang D, Li B, Wang S, et al. Engineered inhaled nanocatalytic therapy for ischemic cerebrovascular disease by inducing autophagy of abnormal mitochondria. *NPJ Regenerative Med*. 2023;8(1):44.
- Zuo D, Tan B, Jia G, et al. A treatment combined prussian blue nanoparticles with low-intensity pulsed ultrasound alleviates cartilage damage in knee osteoarthritis by initiating PI3K/Akt/mTOR pathway. *Am J Transl Res*. 2021;13(5):3987–4006.
- Zhu Q, Guo Y, Chen S, et al. Irinotecan induces autophagy-dependent apoptosis and positively regulates ROS-related JNK- and P38-MAPK pathways in gastric cancer cells. *Onco Targets Ther*. 2020;13:2807–17.
- Zhang H, Zhou Y, Wen D, et al. Noncoding RNAs: master regulator of fibroblast to myofibroblast transition in fibrosis. *Int J Mole Sci*. 2023;24(2).
- Yang C, Zhang L, Huang H, et al. Alantolactone inhibits proliferation, metastasis and promotes apoptosis of human osteosarcoma cells by suppressing Wnt/ $\beta$ -catenin and MAPKs signaling pathways. *Genes Diseases*. 2022;9(2):466–78.

33. Kumar S, Jain A, Choi SW, et al. Mammalian Atg8-family proteins are upstream regulators of the lysosomal system by controlling MTOR and TFEB. *Autophagy*. 2020;16(12):2305–6.
34. Kumar S, Jain A, Choi SW, et al. Mammalian Atg8 proteins and the autophagy factor IRGM control mTOR and TFEB at a regulatory node critical for responses to pathogens. *Nat Cell Biol*. 2020;22(8):973–85.

### **Publisher's Note**

Springer Nature remains neutral with regard to jurisdictional claims in published maps and institutional affiliations.